Engineering Geology 301 (2022) 106618

Contents lists available at ScienceDirect

Engineering Geology

journal homepage: www.elsevier.com/locate/enggeo

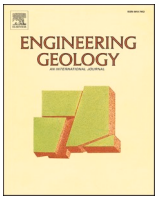

Control of natural fractures in historical quarries via 3D point cloud analysis

Adrián Riquelme [a,*], Javier Martínez-Martínez [b], Iván Martín-Rojas [c], Roberto Sarro [b], Álvaro Rabat [a]

[a] Department of Civil Engineering, University of Alicante, Spain
[b] Instituto Geológico y Minero de España (IGME-CSIC), Calle Ríos Rosas, 23, 28003 Madrid, Spain
[c] Departamento de Ciencias de la Tierra y del Medio Ambiente, University of Alicante, Spain

ARTICLE INFO

Keywords:
Historical quarry
Remote sensing
LiDAR
SfM
RPAS
Natural fractures

ABSTRACT

This paper applies remote sensing techniques and 3D point cloud (3DPC) analysis to the study of historical quarries and the relationship between old quarry landscapes and the natural fracture systems of rock massifs. Ancient quarry landscapes present particular characteristics and different features from those of modern quarries. Consequently, specific considerations are needed when historical extractive places are studied. The proposed method is based on terrestrial 3D laser scanners and the structure from motion technique with remotely piloted aircraft systems. Additional specific fieldwork is required to identify and characterise quarry faces from old, blurry outcrops. A case study of the 18th century "Rambla Honda" quarries in La Romana (Alicante, SE Spain) is presented. The comparison between the fieldwork and 3DPC analysis enables the numbers and orientations of both (1) the discontinuity sets within the rock mass facilitating extraction and (2) the planes resulting from block extraction (traditional quarry faces) to be determined. The comparative analysis reveals how the stonecutters managed the extraction. The results show that structural and stratigraphic discontinuities act as planes of weakness for block extraction and determine the optimum orientation of the quarry face for minimising efforts and rock waste. The final quarry landscape is formed from the superposition of natural and artificial surfaces, but currently they appear eroded and partially covered by silting and plants. The proposed methodology contributes to distinguishing both natural and artificial discontinuities and to achieving a comprehensive knowledge of these cultural places.

1. Introduction

Identifying the natural fracture sets of a rock mass (i.e., joints, fissures, bedding planes, etc.) constitutes a key issue in the development of a quarry, as natural fractures determine both the dimensional properties of the stone blocks and the rational direction in which to advance the mining front during operation (Levytskyi et al., 2017). The presence of discontinuities in a rock volume may lead to the abandonment of a particular quarry face or even the closure of a quarry because they condition both the maximum block size and the amount of waste (Bianchi Fasani et al., 2013). Hence, prior analysis of the fracture set helps to optimise the production of stone blocks (Donnelly, 1979; Fant, 2012; Mosch et al., 2011; Scard, 1989; Stanier, 1985).

Traditional methods for studying the fracture system of a rock massif include theodolites and compass clinometers (Luhmann et al., 2019) and measuring tapes (Einstein et al., 1983; Priest and Hudson, 1981; Priest and Hudson, 1976). These traditional methods require the user to have sufficient experience in deciding where to measure a distance or an orientation. Accordingly, the International Society from Rock Mechanics (ISRM) has suggested several methods for such fieldwork (ISRM, 1978). However, the collection of datasets depends on illumination, accessibility, weather conditions and other factors (Riquelme, 2015).

The rapid development of remote sensing techniques has enabled the application of digital image analysis to sites with natural stone fracture sets, the identification of discontinuity sets (DS) (Slob et al., 2010) and their geometric characterisation (Koch et al., 2017; Martínez-Martínez et al., 2017; Medina-Cascales et al., 2019; Riquelme, 2015). In recent decades, several remote sensing techniques have become powerful tools for geoscientists, enabling them to establish 3D digital models of outcrops to determine their geological structure (Jaboyedoff et al., 2012;

* Corresponding author.
E-mail address: ariquelme@ua.es (A. Riquelme).

https://doi.org/10.1016/j.enggeo.2022.106618
Received 31 August 2021; Received in revised form 8 March 2022; Accepted 9 March 2022
Available online 13 March 2022

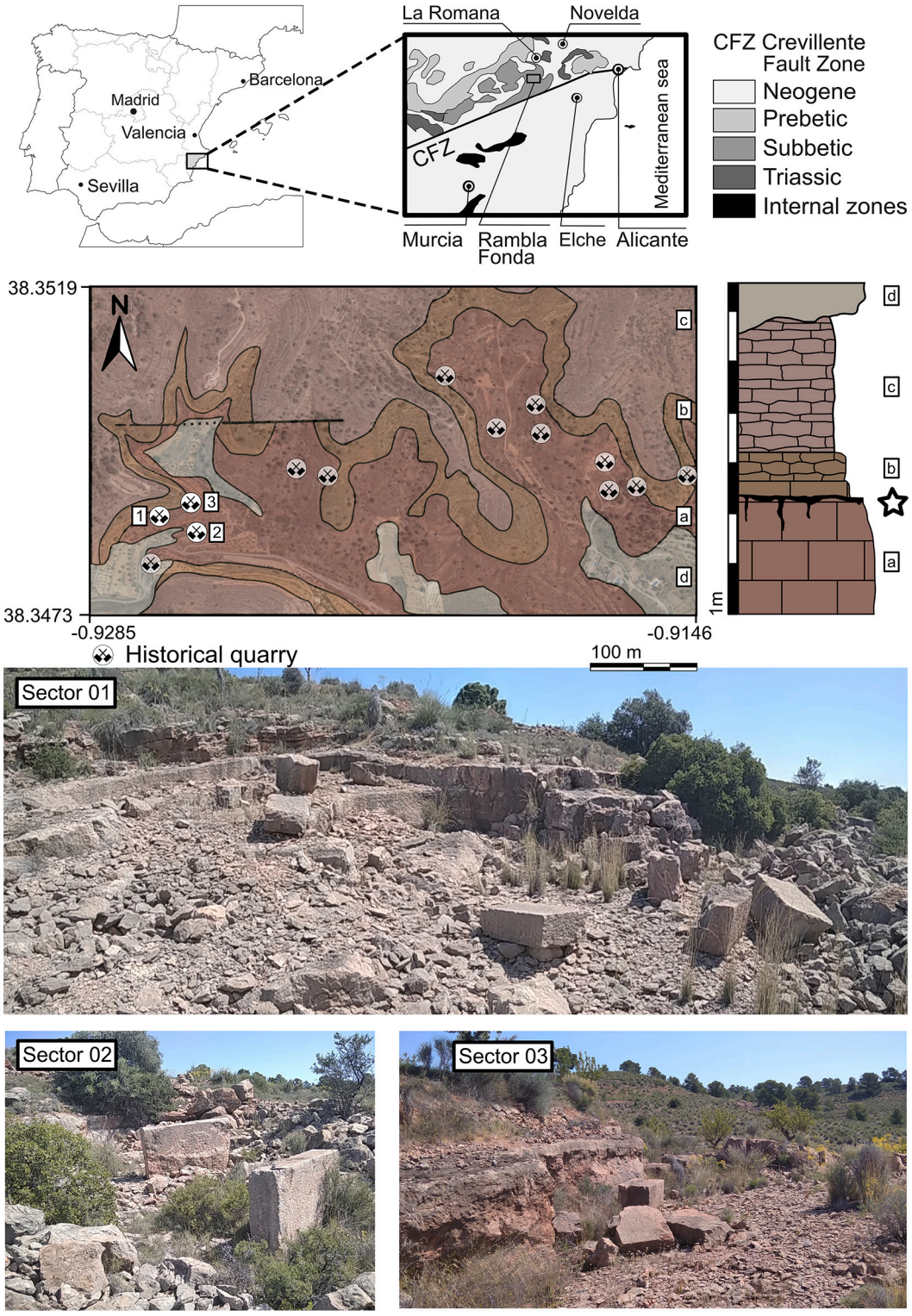

Fig. 1. Geographical and geological context of the studied quarries (adapted from (Martínez-Martínez, 2020)). The historical quarries labelled 01, 02 and 03 correspond to the studied sectors. The letters in the stratigraphic column and geological map are (a) massive red limestone; (b) compacted red nodular limestone; (c) nodular red marly limestones; and (d) Quaternary breccia. The star shows the stratigraphic position of the Fe—Mn oxide crust. (For interpretation of the references to colour in this figure legend, the reader is referred to the web version of this article.)

Vasuki et al., 2014). In this context, the structure from motion (SfM) technique has become a versatile technique, especially when combined with multirotor remotely piloted aircraft systems (RPASs), which can image outcrops from a diverse range of perspectives (Niethammer et al., 2012; Smith et al., 2009; Stumpf et al., 2013). Another powerful tool is ground-based light detection and ranging (LiDAR) also known as terrestrial laser scanning (TLSs), which can capture the coordinates of a scanned surface at high resolution (up to 10^4 points/m^2) and high accuracy ($\sigma < 1$ cm at 100 m). These coordinates are presented as a list of point coordinates or a 3D point cloud (3DPC). The working range of

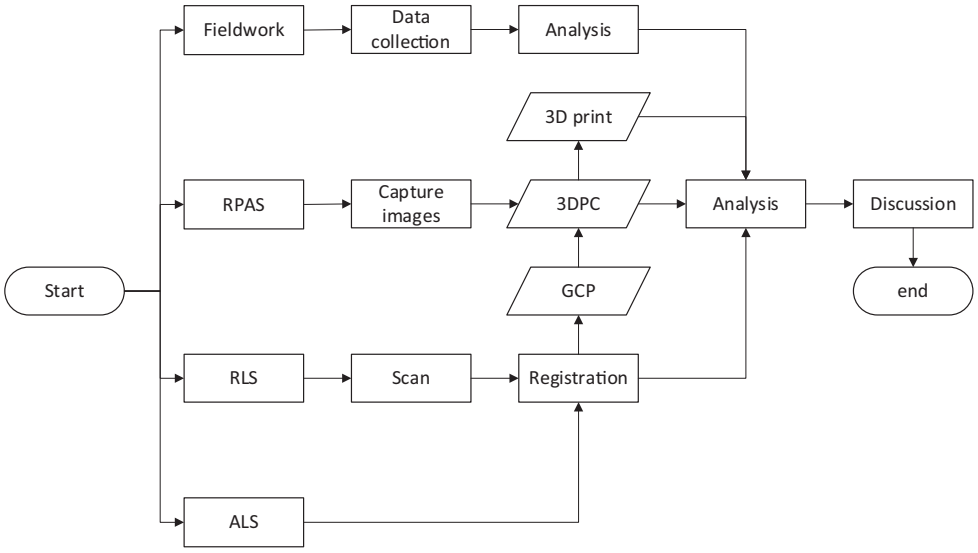

Fig. 2. Workflow of the proposed method.

these tools usually varies from 5 m to 6000 m but depends on the instrument. Both techniques provide a 3D reconstruction of the surface. Therefore, the analysis of these 3D datasets with existing techniques enables the detection of sets of planes, their orientations (García-Sellés et al., 2011; Riquelme et al., 2014a; Slob et al., 2005; Vöge et al., 2013), their shapes (Assali et al., 2014), spacing (Assali et al., 2014; Riquelme et al., 2015), and other characteristics (Riquelme et al., 2018; Sturzenegger and Stead, 2009).

Remote sensing techniques and 3DPC analysis have been applied to active modern quarries to optimise technological mining parameters and improve the quality of the extracted stone blocks (Levytskyi et al., 2018; Mosch et al., 2011). However, they have not been applied to the study of historical quarries. Old quarry landscapes present particular characteristics and different features from those of modern quarries. On the one hand, old quarry faces are frequently smaller and less continuous than those of active quarries. On the other hand, the rock weathering, erosion, plant growth and silting of old quarry landscapes sometimes make it difficult to recognise ancient quarry faces as well as to distinguish them from natural scarps. Consequently, a new specific application of remote sensing techniques to historical quarries is required in order to verify their viability and their strong and weak points.

The geometry, morphology, position, and orientation of ancient and historical quarries are typically studied from a qualitative point of view. In most cases, the quarry typology is classified according to its geographical position in the landscape and the extraction system that was used (Anna Gutiérrez, 2011). In other cases, inactive quarries are classified according to the morphology and typology of the stone resource (Heldal, 2009). Occasionally, the relationship between ancient quarry faces and natural fracture systems has been studied, but only in a descriptive way (Grenne et al., 2014). Consequently, a quantitative approach to the study of historical quarry landscapes is needed to improve our knowledge of these cultural places. Moreover, the application of remote sensing techniques and 3DPC analysis to the relationship between the historical quarry landscape and the natural fracture system of the rock massif can help us understand the quarry management of mining and determine how stonecutters redirected quarry faces to minimise efforts and optimise the utilisation of natural discontinuities.

The aim of this paper is to establish a method for analysing the spatial relationships between natural fracture sets and quarry faces in ancient quarries through the combination of (1) traditional fieldwork and (2) two remote sensing techniques. The new method is applied to the historical quarries of Rambla Fonda (Alicante region, SE Spain), where a highly valuable red limestone has been mined since at least the 18th century. The proposed method is based on the numerical processing of 3DPCs, and it constitutes a novel step in the comprehensive study and understanding of historical quarries.

2. Case study

Over ten small quarries are distributed along a narrow valley (Rambla Fonda valley) 5 km southwest of the town of La Romana (Alicante, SE Spain) (Fig. 1). Geographically, these quarries are between the El Rollo quarry, which was nationally renowned for several centuries, and the modern and active Cavarrassa quarry, from which the commercial building rock 'Rojo Alicante' is currently extracted.

These Rambla Fonda quarries constitute an extensive open cast extraction system (Bessac, 2003) where scattered small fronts in terraces are dispersed throughout a broad area (Fig. 1). This extraction system formed in response to the type of exposure of the stone resource in the landscape: a layer outcropping at a mid-height cape on the side of a valley (a 'layer open-partially covered' exposure according to Heldal (2009)). The production evidence observed in the Rambla Fonda quarries shows that the main technique involved in the extraction of blocks from the bedrock was channelling (Heldal, 2009), thus, unfinished longitudinal sections of channels can still be observed. These channels were made by removing the rock mass via chiselling and/or picking in combination with levering in natural cracks.

The first written references about the Rambla Fonda quarries have been dated to 1764 (Martínez-Martínez, 2020). The 18th century was an active period in all these quarries, and historical references assert that columns and blocks from this extractive area (El Rollo) were used in the Murcia cathedral and even in the Royal Palace of Madrid (1735–1764). The Alicante region is currently one of the most relevant areas in terms of both the extraction and the manufacturing of building stone and ornamental stone at an international level. The industrialisation of different quarries took place during the second half of the 20th century (Martínez-Martínez, 2020). However, most of the Rambla Fonda quarries were abandoned during preindustrial times. Thus, the area contains a large number of diverse in situ remnants of manually worked quarries, which exhibit tool marks on both quarry faces and blocks, broken and half-finished products and work areas in different stages of production (Fig. 1).

Geologically, the quarried layers correspond to the Middle-Upper Jurassic deposits (Upper Ammonitico Rosso Formation) of the External Subbetic Zone (External Zones of the Betic Cordillera) (Fig. 1)

Table 1
Targets used as GCPs: errors of the SfM workflow from Agisoft Metashape (Agisoft, 2019).

Label	X error [cm]	Y error [cm]	Z error [cm]	Total [cm]	Image (pix)
1	−0.434	−1.201	−0.308	1.313	0.755
2	−0.414	−0.874	−0.523	1.1	1.049
3	0.196	−1.966	−0.429	2.021	1.548
4	−0.707	0.864	0.229	1.139	0.876
5	0.307	2.166	0.764	2.318	0.91
6	5.516	7.577	1.647	9.516	1.384
7	−0.73	−2.413	0.212	2.529	0.971
8	−1.301	−1.285	−0.174	1.836	0.862
9	−1.236	−1.39	−0.17	1.868	1.087
10	−1.198	−1.479	−1.247	2.275	1.445
Total	1.913	2.837	0.746	3.502	1.118

(Nieto et al., 2012). The simplified stratigraphic section of the studied deposit, with an average thickness of 60 m, is shown in Fig. 1; the quarry work was focused on the lower member of this sequence, which is a massive red limestone. The microfacies of these rocks are wackestone to packstone with 'filaments' that Reolid and Nieto (2010) attribute to *Bositra buchi*, other allochems are peloids, sponge spicules, crinoids, radiolarian and foraminifera. In the studied zone, an Fe—Mn oxide crust, 2–3 cm thick, is observed at the top of this member. The upper member of the Upper Ammonitico Rosso Formation comprises marly nodular red limestones and red nodular limestones with *Globuligerina* and *Saccoccoma* mudstone–wackestone microfacies, respectively (Reolid and Nieto, 2010).

3. Method

3.1. Three-dimensional point clouds acquisition

The proposed method enables a surface analysis of a quarry to detect the DSs along the extraction surfaces that are not necessarily parallel to the discontinuities. Fig. 2 shows the overall workflow for obtaining information about the DSs or natural fractures, and the planes resulting from block extraction. The fieldwork is performed by an experienced user to collect measurements of the DS orientations and analysed using traditional methods (ISRM, 1978; Rocscience, 2021). In addition, the surface is captured using remote sensing techniques. In this work, we used TLS instruments and the SfM multiview stereo (SfM-MVS) technique.

Setting up the area to scan comprises the placement of targets between the TLS stations to serve as common points. These targets provide coordinates that serve as ground control points (GCPs) for the SfM workflow (Riquelme et al., 2017). The first step is to capture the surface

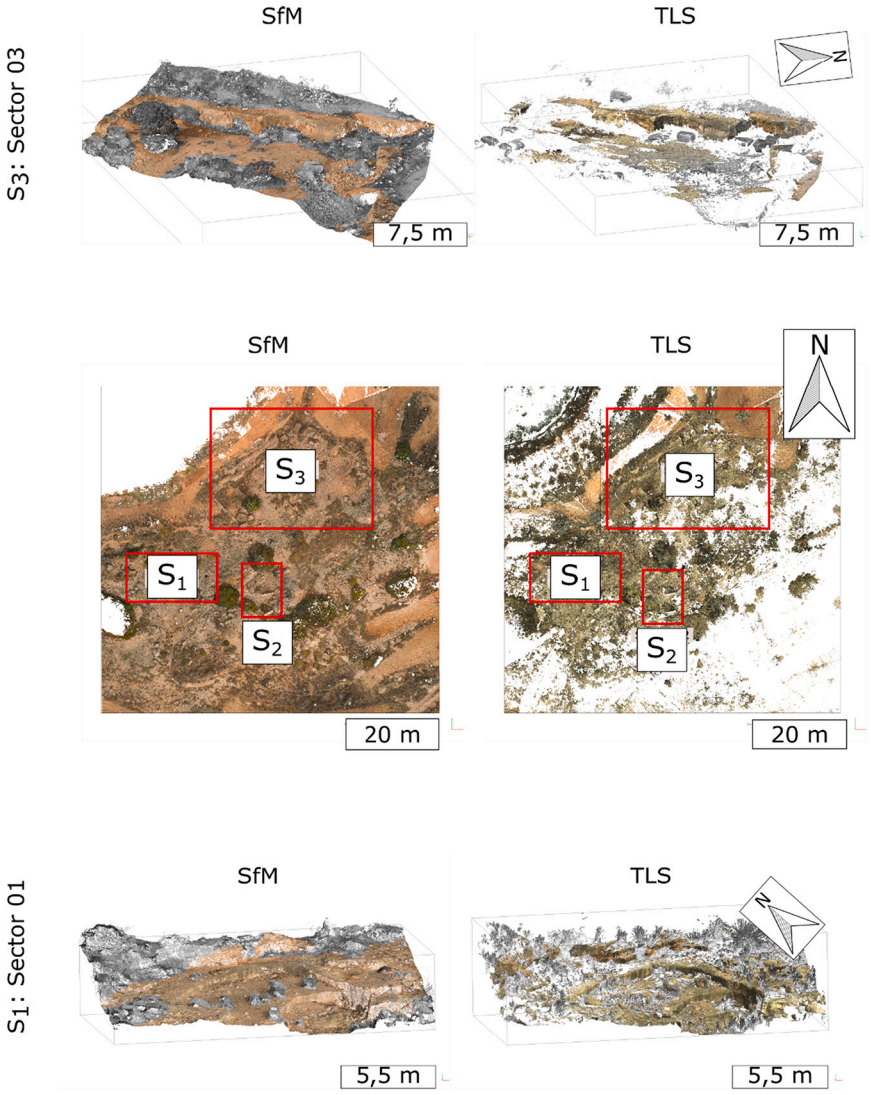

Fig. 3. Orthographic views of the 3DPCs generated via SfM and TLS (ground points are coloured, discarded points are depicted in grey).

using the TLS instrument. During scanning, the coordinates of the targets are captured in a local reference system, denoted TLS-3DPC. Then, a georeferenced airborne laser scanner (ALS) 3DPC is downloaded from the open-source National Plan for Aerial Orthophotography (Plan Nacional de Ortofotografía Aérea PNOA) Project (Instituto Geográfico Nacional de España, 2016a, 2016b). To obtain the 3DPC and the target coordinates in a global reference system, denoted ETRS89 30 N, a 3-axis translation and an OZ-axis rotation are applied using the ALS-3DPC as the reference. However, if TLS-3DPC is not levelled, the rotation should not occur around only the vertical axis, rather the rotation should involve all three axes. This step provides the georeferenced TLS-3DPC and target coordinates. In this work, we used a Leica C10 ScanStation 3D laser scanner (Leica Geosystems, 2011). Seven scan stations were used, and there were ten . The targets were used to roughly register the scan stations. Then, the scans were registered using cloud-to-cloud constraints with Cyclone software (Leica Geosystems, 2021), and the overall error was 1 cm.

The SfM process begins with the capture of photographs. In this work, we used an RPAS equipped with an FC300S camera (focal length of 3.61 mm, equivalent to a 20 mm lens on a full-frame 35 mm camera). The photograph resolution is 4000 × 3000 pixels, and the photographs capture both the surface and the targets. The global coordinates are inserted into the SfM workflow, so the SfM-3DPC-referenced dataset is scaled and georeferenced to TLS-3DPC. The bundle adjustment error is shown in Table 1. Since both the TLS and the SfM datasets are registered, scaled, and oriented, both 3DPCs can measure orientations and lengths.

3.2. Analysis of the surface

To analyse the orientations of the planes observed on the rock surface, the 3DPCs were analysed using Discontinuity Set Extractor (DSE) software (Riquelme et al., 2016; Riquelme et al., 2014a). This software analyses all the points of a 3DPC and calculates the normal vector for every point using the k-nearest neighbour algorithm (where k is established by the user, usually 30 (Riquelme et al., 2014b)). All the resulting normal vectors are plotted on a stereonet by their corresponding poles; since 3DPCs can contain millions of points, millions of poles are plotted on the stereonet. Since it is nearly impossible to visually identify sets of poles because of their immensely large number, the density of the poles is calculated using the kernel density estimation (KDE) technique (Botev et al., 2010). A concentration of poles in a certain stereonet region reflects a set of points with a similar orientation. This orientation can be interpreted as a random surface, a mining face within the quarry, or an actual DS. The software, however, does not make this distinction because it only analyses the geometry.

Instead, the user supervises and decides how many DSs there are and defines their orientations. For every point, if a certain set of geometrical requirements is satisfied (Riquelme et al., 2014a), a DS is assigned; if not, the point is left unlabelled and is not considered. Then, cluster analysis is performed (Ester et al., 1996) to arrange all the points of a DS along parallel planes and determine their best-fit equations. This provides a classified point cloud that enables the normal spacing to be estimated (Riquelme et al., 2015) and the persistence among these discontinuities to be analysed (Riquelme et al., 2018).

It is worth noting that the analysis of 3D datasets cannot determine whether a DS is a set of natural fractures or the face of a quarried block. However, fieldwork data are collected when a plane is considered a discontinuity that continues within the rock mass. Because of this, the combination of fieldwork information with classified 3DPC information enables the analysis, interpretation, and discussion of whether the detected orientations belong to a quarry face or to a natural fracture. In addition to this differentiation, the relations between orientations enable us to investigate how natural fractures governed the extraction of blocks from the quarry.

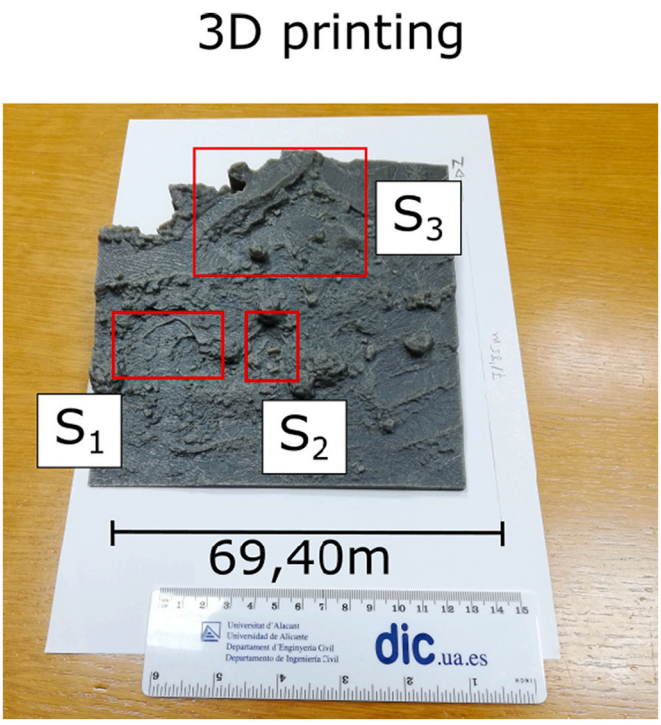

Fig. 4. 3D printing result from the SfM mesh, and detailed views of the two analysed quarries.

4. Results

In this work, TLS and an RPAS enabled the generation of two 3DPCs. In addition, the SfM workflow generated a 3D mesh, and a 3D printer generated a scaled 3D object, as shown in Fig. 3. This 3D object was useful for interpreting the main orientations jointly with the rest of the results because it was scaled and oriented towards north. As expected, the captured SfM surface covered the entire surface of the study area with fewer areas of missing data than the TLS surface because the RPAS captured the whole study area. In contrast, TLS instruments work with a subhorizontal laser beam, so most (but not all) of the areas of interest were scanned. (See Fig. 4.)

The TLS and SfM workflows were performed simultaneously, and the working time was approximately three hours. Both datasets were processed to generate the corresponding 3DPCs. Registering, georeferencing and extracting the targets from the TLS data took approximately four hours. Then, the SfM processing time was approximately two hours using a 32 GB i7–4790 Intel processor equipped with an Nvidia GTX-1650 graphics card. The removal of vegetation took over three hours for both datasets.

Quarry activity was observed in three sectors, as shown in Fig. 3. Sectors 01 and 03 were both wide enough to be studied using the traditional methods and to be captured by the TLS and the RPAS. However, Sector 02 was too narrow, and it was covered by debris and blocks, making it impossible to study without removing the debris. Accordingly, Sector 02 was not analysed, and detailed analyses were performed on Sectors 01 and 03, which exhibited more appropriate conditions for the numerical simulation (Fig. 3; corresponding areas marked in red rectangles).

The analysis results of Sector 01 are presented in Figs. 5 and 6 for the SfM and TLS datasets, respectively. Likewise, the Sector 03 results of the SfM and TLS datasets are shown in Figs. 7 and 8, respectively. As previously mentioned, noise, vegetation, and abandoned blocks were removed from the 3DPCs. After the data were cleaned, the points were subsampled to 1 cm to enhance the density of the normal vector poles.

In particular, the SfM dataset of Sector 03 showed that the

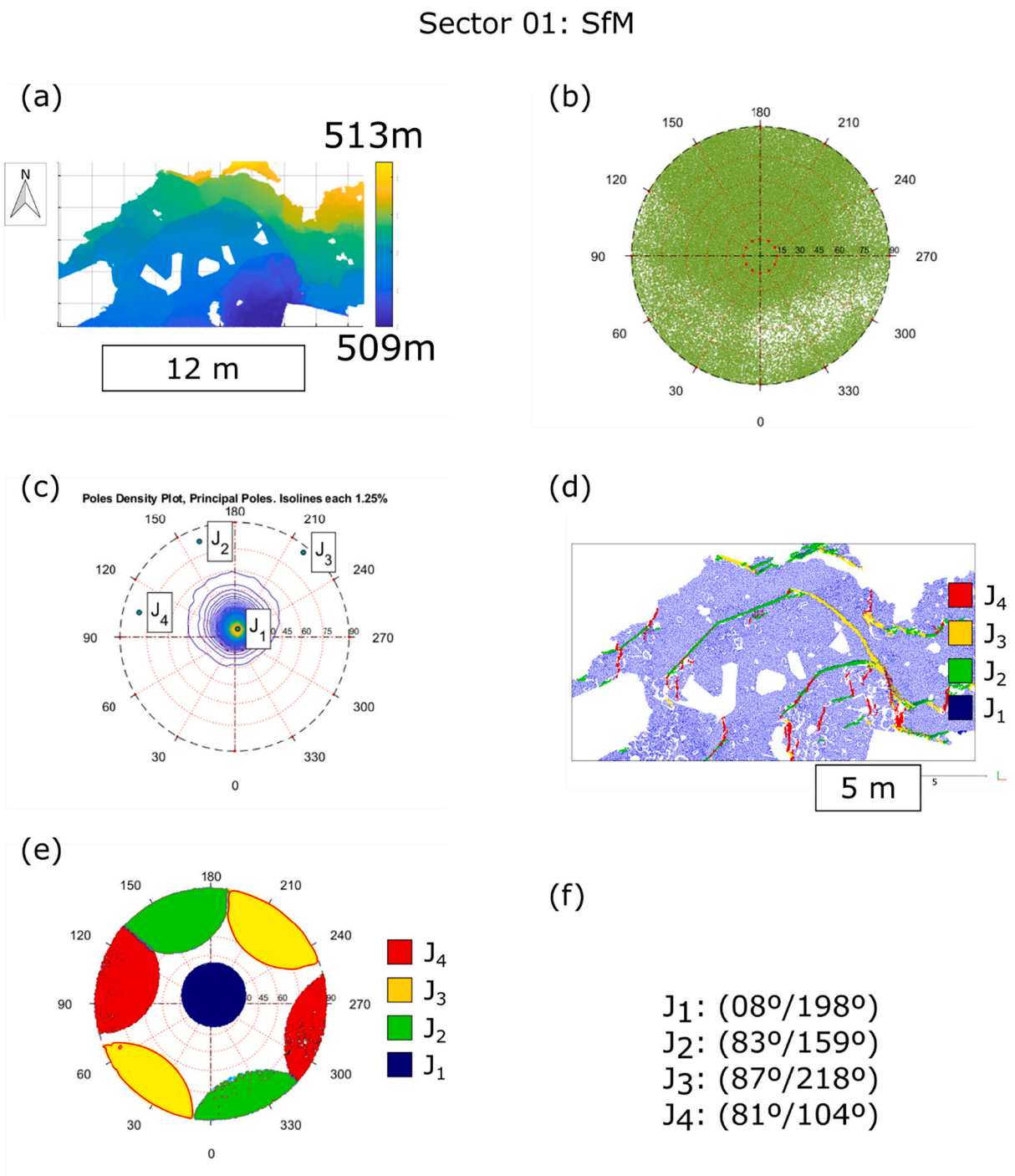

Fig. 5. Extraction of the orientations of Sector 01 via the SfM-derived 3DPC: (a) elevation map; (b) stereonet of the 774.861 normal vector poles; (c) density of the poles and extraction of the principal DS; (d) top view of the classified 3DPC; (e) stereonet of the 647.750 poles assigned to the corresponding DS; (f) orientations of the principal DS.

subhorizontal surface (i.e., the bedding plane corresponding in this case to the ground) was wider than the subvertical surfaces. In addition, the ground was covered by debris, so in terms of this analysis, it was a noisy plane. The normal vectors of these points were not concentrated around their mean orientation but were sparse on the stereonet, leading to interference with other DSs during the analysis. Therefore, to analyse the subvertical surfaces (which were expected to have affected the extraction of blocks), the SfM-derived 3DPC was further processed: the (04 ° /225°) bedding plane was extracted, and those points were removed.

In Figs. 5 through 8, subfigure (a) presents a top view of the corresponding 3DPC. For every point, the 30 nearest neighbours were detected, and the normal vector was calculated for that set and assigned to the corresponding point. The normal vector was converted to its pole and plotted on a stereonet, as shown in subfigure (b). These figures show that, as mentioned above, the number of measurements is considerable, and thus, they cover most of the stereonet. The results of the statistical analyses performed to detect the orientations of the high-density poles are shown in subfigure (c), which displays the nonparametric function determined via the KDE technique (Botev et al., 2010). In these figures,

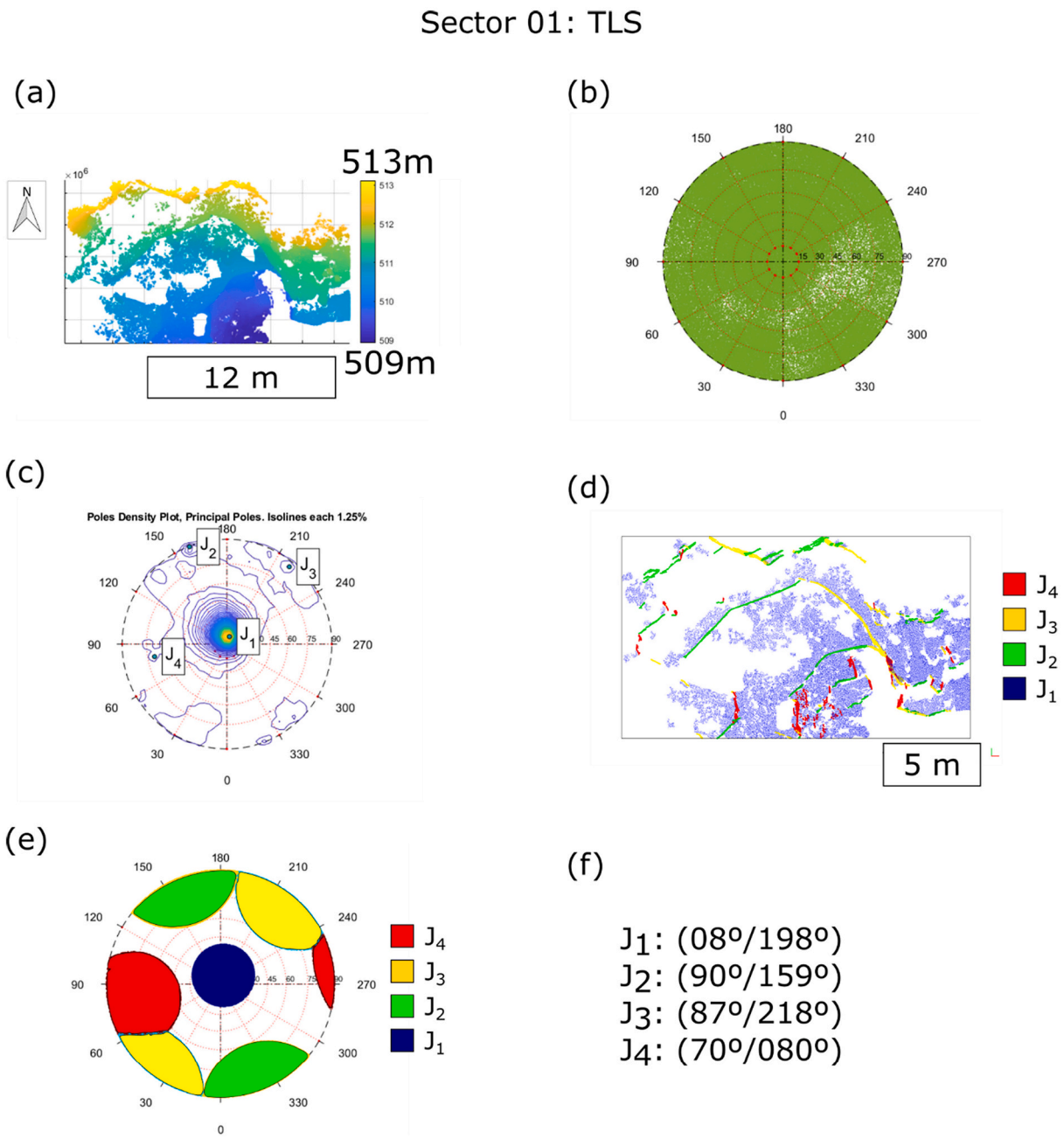

Fig. 6. Extraction of the orientations of Sector 01 via the SfM-derived 3DPC: (a) elevation map; (b) stereonet of the 483.427 normal vector poles; (c) density of the poles and extraction of the principal DS; (d) top view of the classified 3DPC; (e) stereonet of the 368.823 poles assigned to the corresponding DS; (f) orientations of the principal DS.

the maximum values show the principal poles of the main DSs. As shown, four principal orientations were extracted, although the fourth orientation (i.e., J_4) changed depending on the technique used and the studied sector. Subfigure (d) presents the stereonet of the poles given in (b), in which each pole was assigned to the closest DS. In addition, poles with an angle greater than 30° relative to the closest DS were removed. These figures show that the number of points at the end of the analysis was considerably fewer than that in the original point cloud. DSs J_1, J_2, J_3 and J_4 were distinctly coloured blue, green, yellow and red, respectively. Subfigure (e) presents a top view of the classified 3DPC, where every point is coloured according to its assigned DS. Finally, the DS orientations are shown in (f), for which the dip and dip direction angles are given in degrees.

In addition to being subjected to the above 3DPC analysis, the natural fractures and DSs were analysed in the field (Fig. 2). The data measurements captured 67 and 51 orientations for sectors 01 and 03, respectively. To measure the orientations, a smartphone equipped with an accelerometer was used. Fig. 9 presents the results of the analysis using Dips software (Rocscience, 2021).

5. Discussion

5.1. TLS and SfM comparison

In this section, we compare the plane orientations obtained with two digital techniques: TLS and the SfM technique. Figs. 10, 11 and 12 summarise the results of both techniques for Sectors 01 and 03 in combination with the fieldwork results. In Fig. 12, the plane orientations

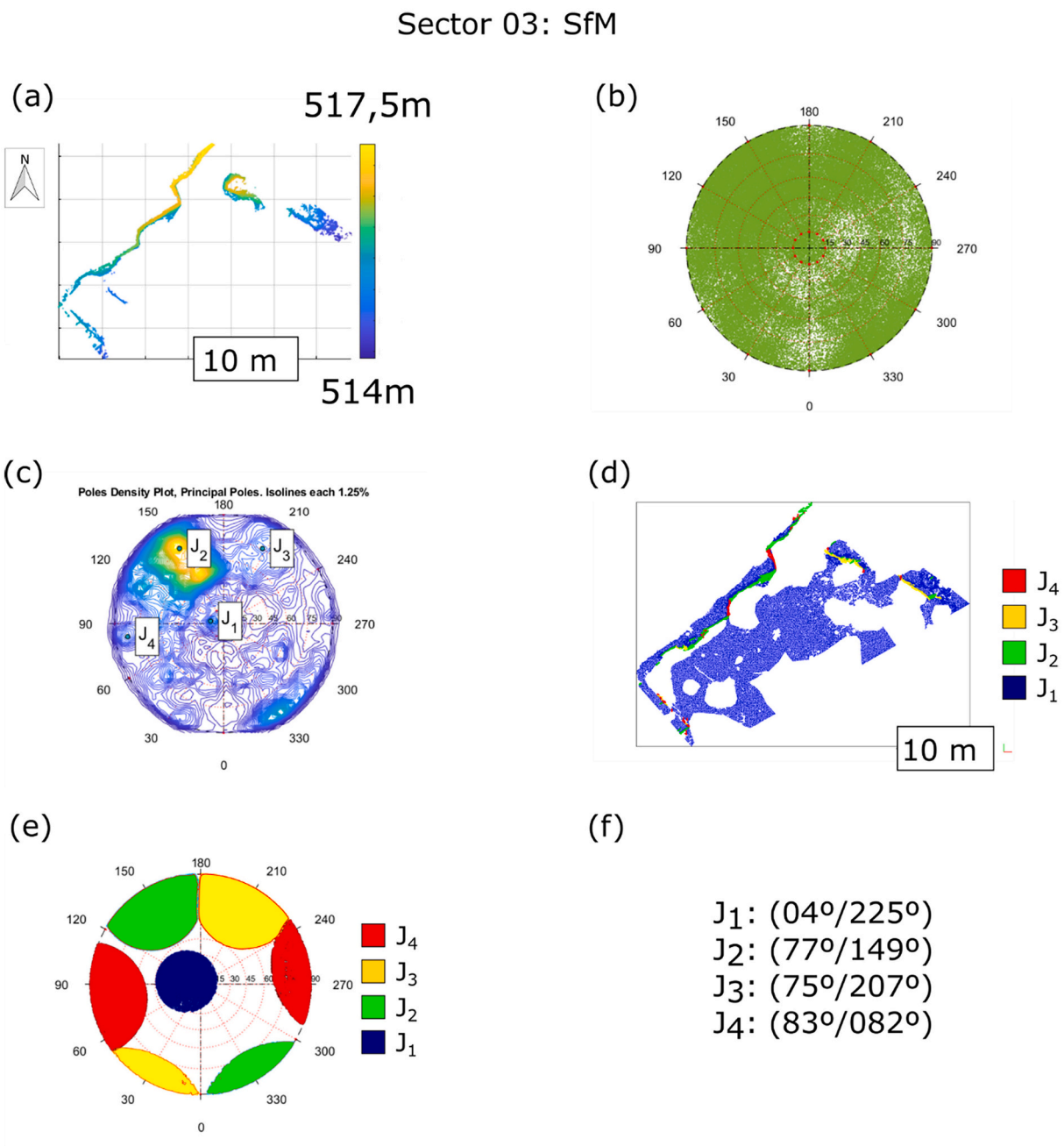

Fig. 7. Extraction of the orientations of Sector 01 via the SfM-derived 3DPC: (a) elevation map; (b) stereonet of the 483.427 normal vector poles; (c) density of the poles and extraction of the principal DS; (d) top view of the classified 3DPC; (e) stereonet of the 368.823 poles assigned to the corresponding DS; (f) orientations of the principal DS.

derived from the SfM and TLS techniques are shown as green diamonds and blue crosses, respectively. In addition, the orientations of the natural fractures (the fieldwork results) are depicted as red crosses.

The automated analysis yielded the first DS, J_1, with a subhorizontal attitude (Fig. 12). A comparison with the hand-collected field data showed that J_1 corresponds to bedding planes and the ground surface within the quarry. The J_1 orientations in the TLS and SfM-derived data are consistent. Figs. 10 and 11 show the classified 3DPCs for both sectors and both techniques; the point members of this DS are coloured in blue. The results demonstrate that this DS is persistent and is the widest DS.

The analysis showed that J_1 is challenging to analyse because of the debris covering the ground. As the sides of debris are oriented randomly, their normal vectors randomly vary around the ground normal vector, leading to scattered poles around the principal pole of the stereonet and masking other trends. This effect was especially disruptive in Sector 03 when the SfM dataset was used. Notwithstanding, the principal orientation determined using the 3DPC matches that determined from the fieldwork.

In addition to J_1, three subvertical orientations (J_2, J_3 and J_4) were detected using the 3DPCs. In the classified point clouds, J_2 is coloured yellow. In addition, the stereonets present the detected poles grouped in a yellow circle for both sectors. For Sector 01, the poles match perfectly, and for Sector 03, there is only a minor variation. The classified point cloud of Sector 01 shows that J_2 is a persistent DS, and its length is greater than 10 m. Sector 03 shows similar results; however, the planes are smaller than in Sector 01, although they are clearly defined.

J_3 is represented in green in both the classified 3DPCs and the stereonets. Although minor orientation differences were detected between

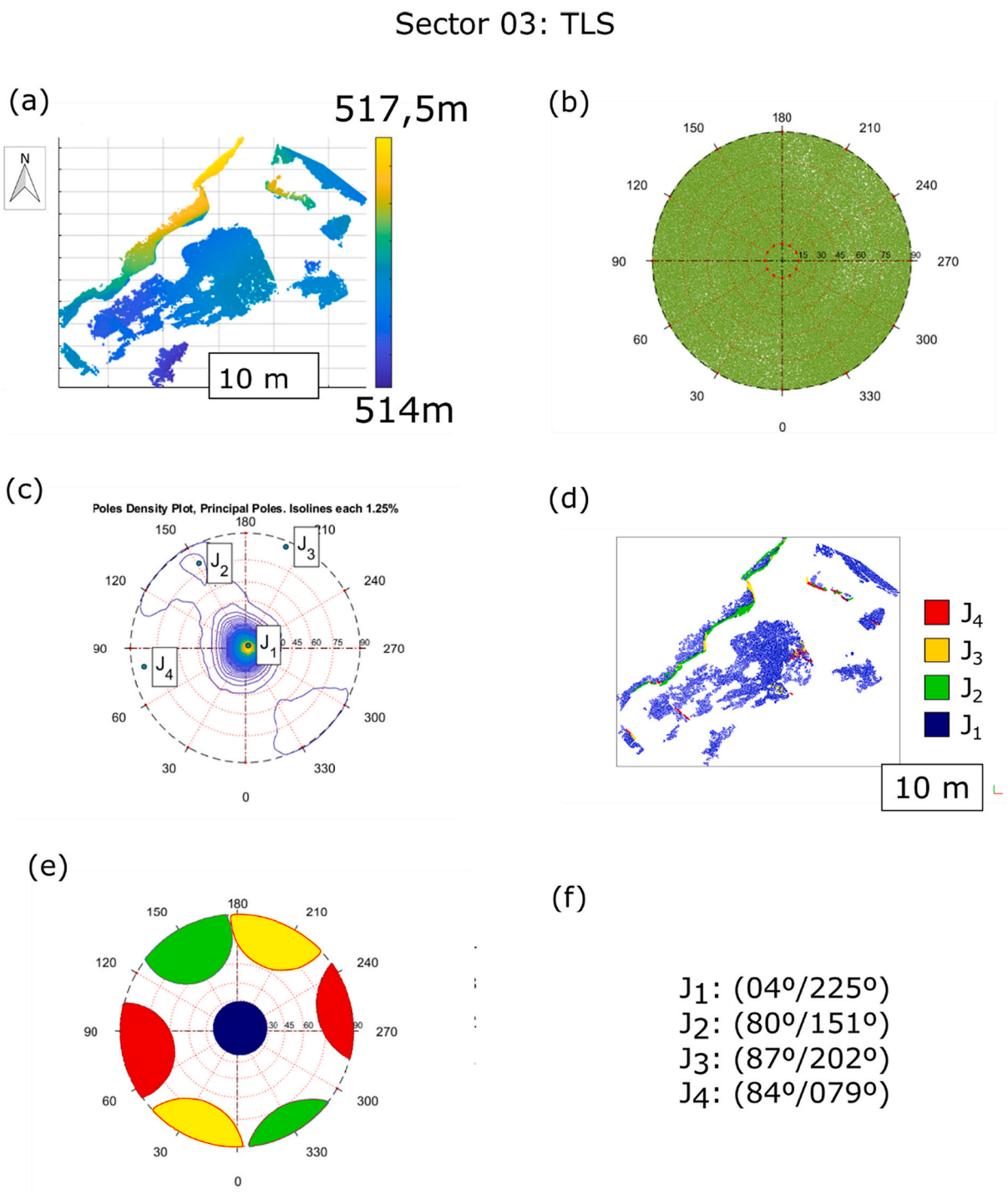

Fig. 8. Extraction of the orientations of Sector 03 via the SfM-derived 3DPC: (a) elevation map; (b) stereonet of the 695.811 normal vector poles; (c) density of the poles and extraction of the principal DS; (d) top view of the classified 3DPC; (e) stereonet of the 487.689 poles assigned to the corresponding DS; (f) orientations of the principal DS.

Sectors 01 and 03, the extracted values using both techniques agree. This wide DS is clearly observed in both sectors.

Finally, the analysis of J_4 using both the TLS and the SfM datasets showed a variation in the strike in Sector 01 and an excellent match in Sector 03. The strike variation found in Sector 01 is explained by the nature of the technique. To understand this variation, let us focus on the classified point cloud of Sector 01 (Fig. 10), where the point members of J_4 are depicted in red. Most of the larger planes match between both techniques, but other smaller planes do not. This is because the techniques reconstruct the 3DPC differently. Some of the orientations of small planes form a small angle with the principal orientation and within the threshold. Accordingly, they are classified as members of this DS, and the principal orientation somehow changes.

The abovementioned orientation variation was also detected on the other DSs. Interestingly, while all the principal poles of J_1 almost match, those of J_2 and J_3 show minor variations depending on the dataset. TLS is a 3D ground-based laser scanning technique; in typical scanners, the laser beam is distributed over a range of 360 degrees horizontally and 270 degrees vertically by a rotating mirror (Tallon, 2014). Therefore, the laser works under optimal conditions when scanning subvertical

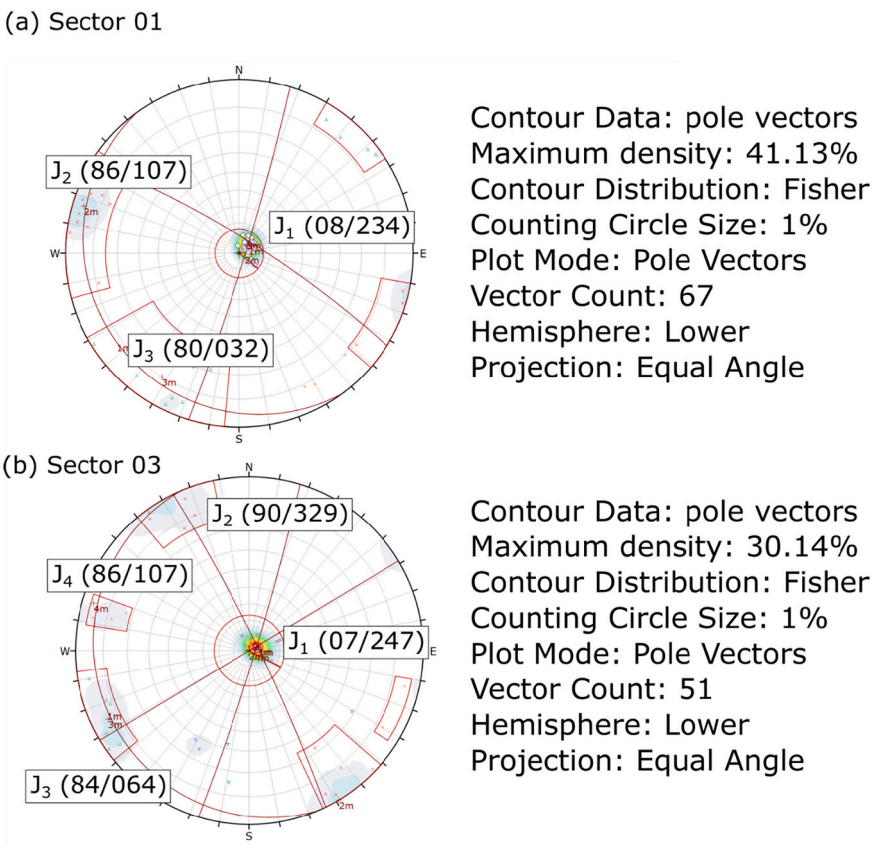

Fig. 9. Fieldwork datasets: stereonet plot and major planes of Sectors (a) 01 and (b) 03.

planes and the laser beam is horizontal (ceilings can also be scanned in excellent conditions, but in open pits, the instrument has no reference). However, scans of the ground are dramatically affected by the angle between the line of sight and the scanned surface with the distance, leading to a lower density of points on the ground (Lato et al., 2010). In contrast, SfM is a technique that processes images, which (in this case) were captured using an RPAS. Therefore, the altitude angle was close to −90° relative to the horizontal. The reconstruction quality of sub-horizontal surfaces is excellent, but that of subvertical surfaces is not; hence, the quality of small subvertical planes differs, affecting the results.

Regardless of whether the plane is an excavation face or a natural DS, the density function of Sector 01 engenders an interesting discussion (Fig. 13). The poles of J_2 are not concentrated at a single point but rather a tight cluster of points. The orientations of J_2 extracted from the TLS and SfM data were (90 ° /159°) and (83 ° /159°), respectively. Another close cluster was detected at (80 ° /135°) (Fig. 13 b), which was found to be an excavation face (Fig. 13 a). The observation of the density function would lead to the recognition of two separate DSs, but after closely inspecting and interpreting the 3DPCs, it was considered a single DS. In fact, it is common to observe subparallel planes in excavated areas that do not correspond to DSs. In these cases, to simplify the analysis, it is reasonable to treat them as a single surface. However, if there is a special interest in their individual analysis, the two orientations can be separated and treated as different DSs.

According to the presented results, both techniques can provide excellent results for detecting the attitudes of plane with similar orientations. Notably, these planes can be detected regardless of their origin. As stated before, when dealing with ancient open pits, these planes are considered excavation faces but can also be natural fractures.

5.2. 3DPC and fieldwork comparison

The aim of this subsection is to determine whether a DS is a natural fracture set or a new face started within the quarry to extract blocks of the desired size and shape.

The orientations obtained from the 3DPCs are considered block excavation faces because they were left when the stone cutter excavated the rock. In addition to these excavation faces, the fieldwork also registered discontinuities within the rock mass that were identified in outcrops (traces on the rock surface) as cracks. When a wide plane was observed but there was no continuity within the rock mass, it was not considered a fissure. To summarise the results, Table 2 shows the detected natural fractures from the fieldwork and the excavation faces detected from the 3DPC analysis.

The first DS, which is the bedding plane, perfectly agrees with the digital datasets and the fieldwork. This is the widest surface and is therefore best represented by the points. This agreement supports the idea that this DS was used as a weak surface to extract the blocks.

DS J_2 was observed by fieldwork in Sector 03 but not in Sector 01. However, the 3DPC analysis detected the orientation of J_2 in both sectors. This means that in Sector 03, J_2 was a natural fracture, and the stonecutter extracted the blocks following its orientation. In contrast, DS J_2 was detected only by 3DPC analysis in Sector 01. We hypothesise that this signifies that the extraction started in Sector 03, where this wide fracture was taken advantage of to extract the blocks. The excavation continued into Sector 01, but as the natural fracture disappeared, the orientation of J_2 was maintained despite the absence of natural fractures within the rock mass to preserve the size and shape of the excavated blocks.

The third DS is J_3. Both the fieldwork and the 3DPC analysis detected this DS in both sectors (Table 2). However, the orientations derived from the fieldwork showed different values. In Sector 01, J_3 showed similar

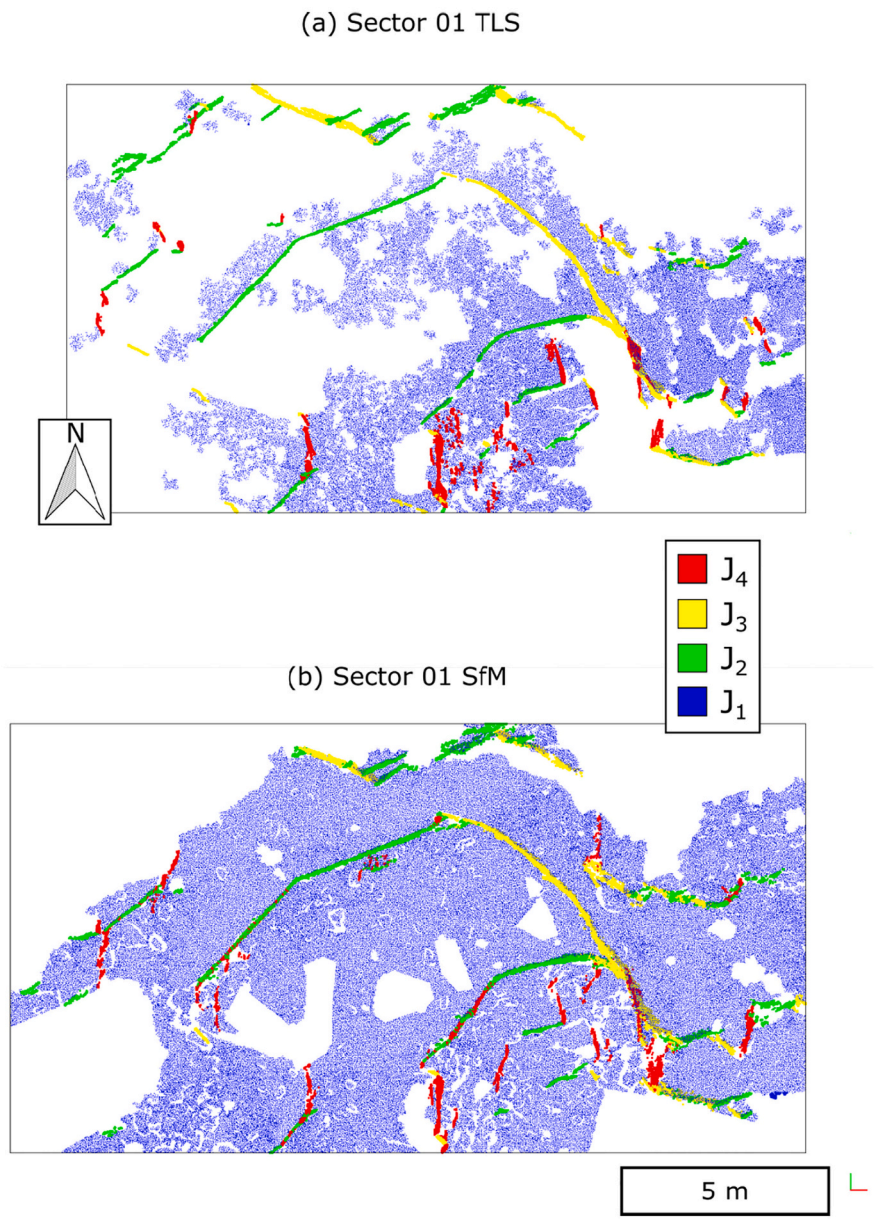

Fig. 10. Comparison of the major orientations for Sector 01. Top views of the classified 3DPC according to the selected DS: (a) TLS and (b) SfM.

strike angles, but as it is a subvertical plane, the dip direction varied by almost 180°. This is a common effect when working with subvertical planes. However, in Sector 03, the J_3 natural fractures identified by the fieldwork presents a different strike angle from that of the 3DPC analysis. A visual analysis of the 3DPC of Sector 03 (Fig. 11) shows that J_3 outcrops are small compared to those of J_1 and J_2. We postulate that the difference in the observed orientations could be related to this fact because the fieldwork measurements were hard to capture, leading to possible deviations. In addition, the similar orientations between the 3DPC results and the fieldwork suggest that the excavation activity meant that the orientation of the J_3 natural fractures was maintained to continue extracting blocks. Interestingly, the stereonet revealed that J_1, J_2 and J_3 form almost right angles. This agrees with the fact that the abandoned blocks were parallelepipeds.

Finally, J_4 was detected in Sector 01, where its orientation matched that determined via the SfM technique but showed minor differences from the TLS result. In Sector 03, both the TLS and the SfM results were fitted, and the fieldwork results were slightly different. Despite the small size of this natural fracture, the classified point clouds show that excavation was similarly conducted using this natural fracture to extract blocks.

5.3. Geoarchaeological interpretation of the 3DPC results

The most significant DS controlling block extraction was J_1. The discontinuities included in this set correspond to bedding planes and frequently occurring stylolites parallel to the stratification structure. Stonecutters used both types of discontinuities as precut basement planes. In addition, the distance between these basal planes determined, in most cases, the height of the final block. Partially cut blocks remain in the quarry areas, showing this preferential orientation favouring the stratification and stylolite planes (Fig. 14 a). We also found some wedge boxes remaining in the faces of these quarries along the surface traces of stylolites (Fig. 14 c). Using these natural discontinuities, planes of weakness for block extraction justify the coincidence between the natural discontinuities and the SfM- and TLS-derived surfaces (Fig. 12).

In addition to the subhorizontal surface, two additional surfaces are needed to produce a rock block. These surfaces must be orthogonal or

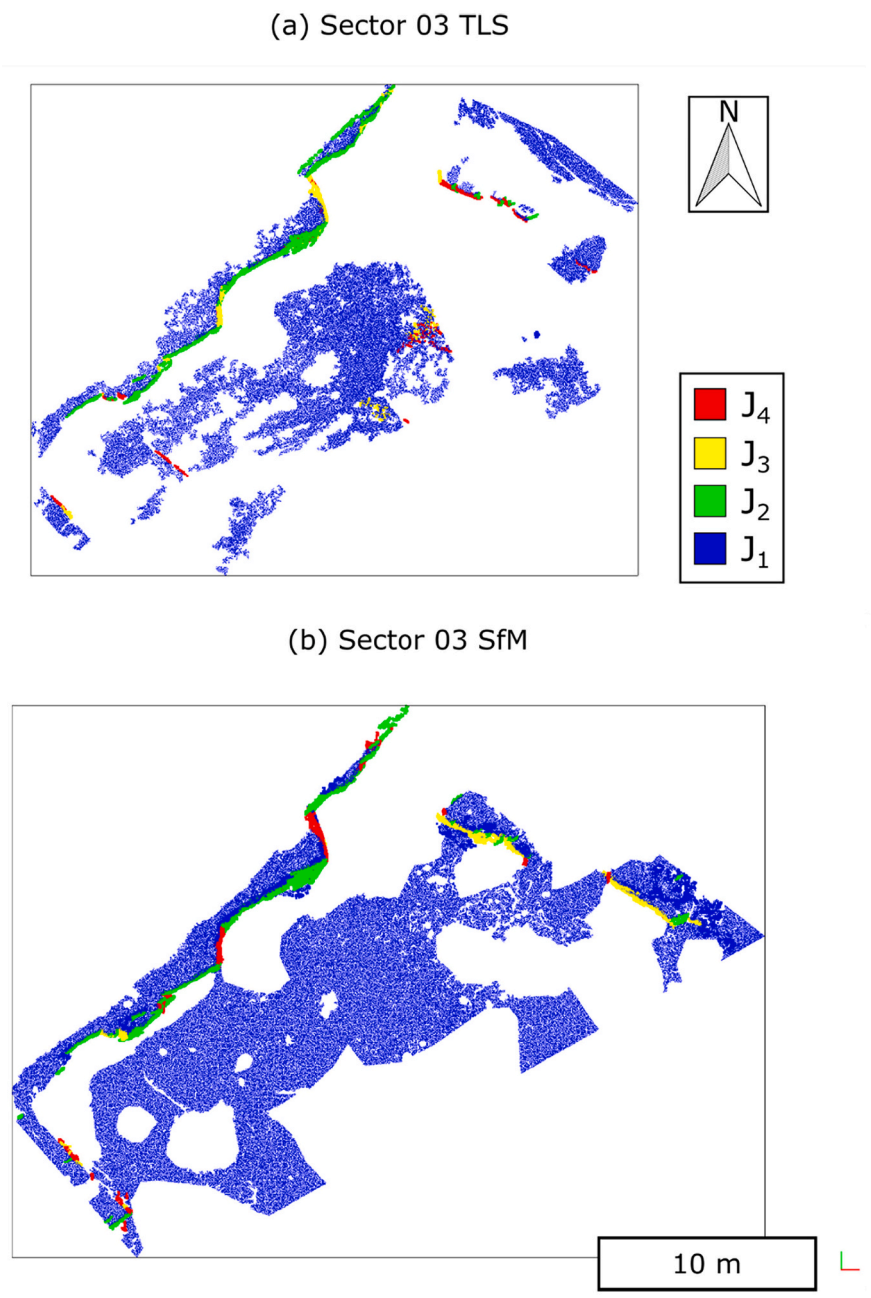

Fig. 11. Comparison of the major orientations for Sector 03. Top views of the classified 3DPC according to the selected DS: (a) TLS and (b) SfM.

nearly orthogonal to obtain pieces with forms close to their final geometry. Under the optimal conditions, natural fractures are used to minimise efforts. However, when the orientation of natural cracks is not appropriate, new discontinuities must be manually opened through pickaxes and/or wedges. The particular situation of the studied historical quarries can be determined from the analysis of the stereonets in Fig. 12. Two natural fracture sets are recognised in Sector 01: one in J_3 and the other in J_4. These two natural DSs intersect at angles of 75–80°. However, J_2 in Sector 01 is formed by only artificial surfaces cut in the rock mass and is at angles of 80–90° from some fractures included in J_4. This situation confirms that new orientations were created by quarry workers, forming an orthogonal net. However, non-parallelepiped blocks were obtained when the block boundaries were defined by natural cracks. In these cases, manual work was subsequently needed to cut the blocks into regular ashlars (Fig. 14 c).

A similar situation was found in Sector 03, where three natural DSs were observed in the rock mass: one in J_2 and the other two in J_4. The natural cracks of J_2 and one set of J_4 form an angle of exactly 90°. A new DS (J_3) was then created at 90° to the second natural set included in J_4 (87°/108°). This sector constitutes an exceptional case study to analyse the influences of natural fractures within a rock mass on the orientation and extraction of rock blocks, prioritising the use of natural cracks and creating new discontinuities orthogonal to the previous discontinuities.

6. Conclusions

The application of the presented method has demonstrated that this is a useful tool in the characterisation of how fractures control the effective extraction of stone blocks from quarries. Analysing the 3DPCs of the studied Rambla Fonda quarries yielded the following conclusions:

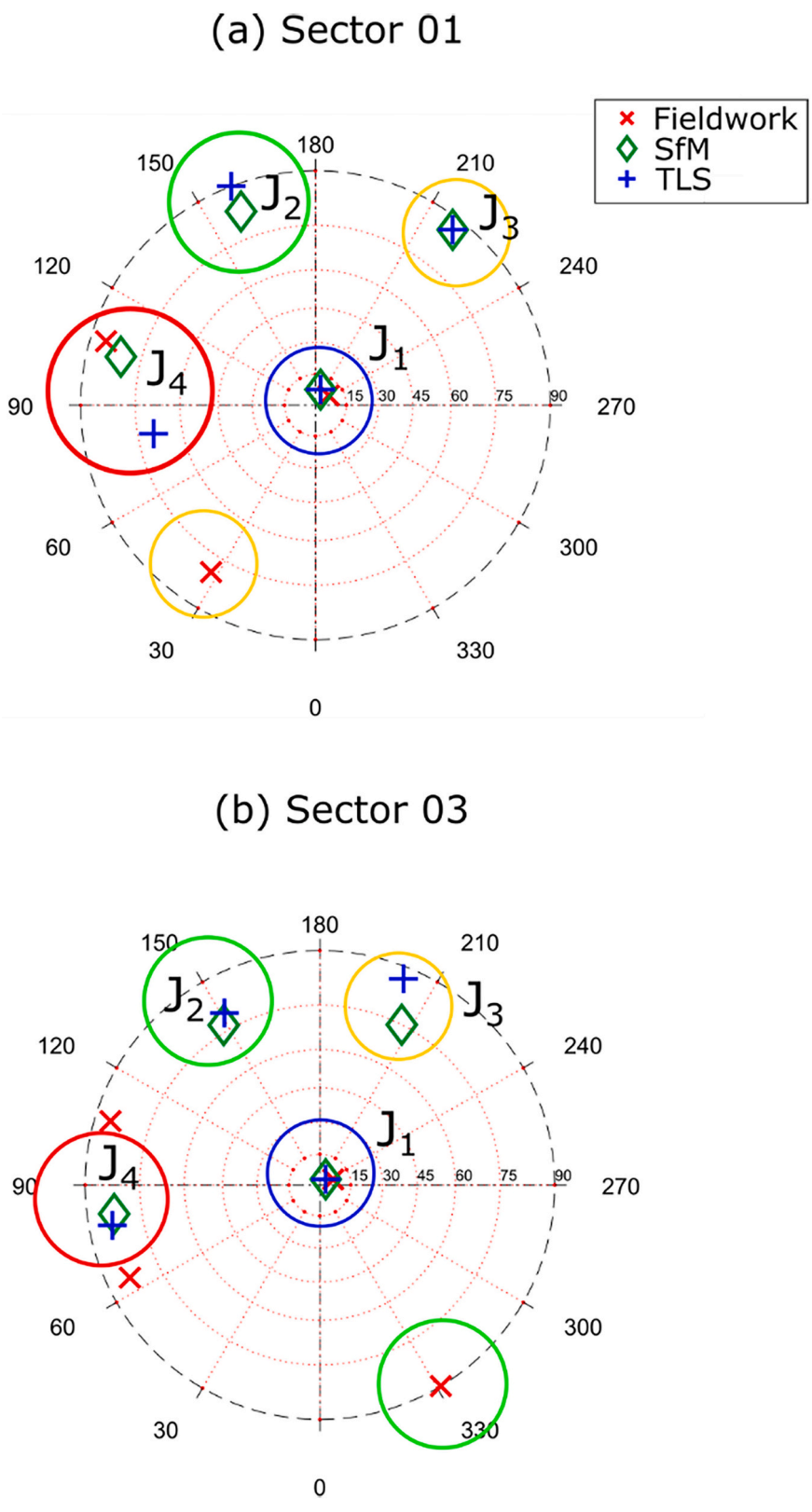

Fig. 12. Comparison of the major orientations for Sectors (a) 01 and (b) 03. The principal orientations from the fieldwork are shown on a stereonet.

1. Stylolites and bedding planes (J_1 set) act as basal planes of weakness for extracting stone blocks. The distance between these basal planes also determines, in most cases, the height of the extracted block.
2. Three additional fracture sets in the historical quarries (J_2, J_3 and J_4) were detected in the 3D point cloud. In some parts of the quarries, one of these fracture families is artificial (J_2 in Sector 02) corresponding to artificial quarry faces forming an orthogonal net with the other natural discontinuities. In another studied sector (Sector 01), the natural fracture sets meet at an angle of exactly 90°, creating the optimum situation and minimising efforts for stone block cutting.

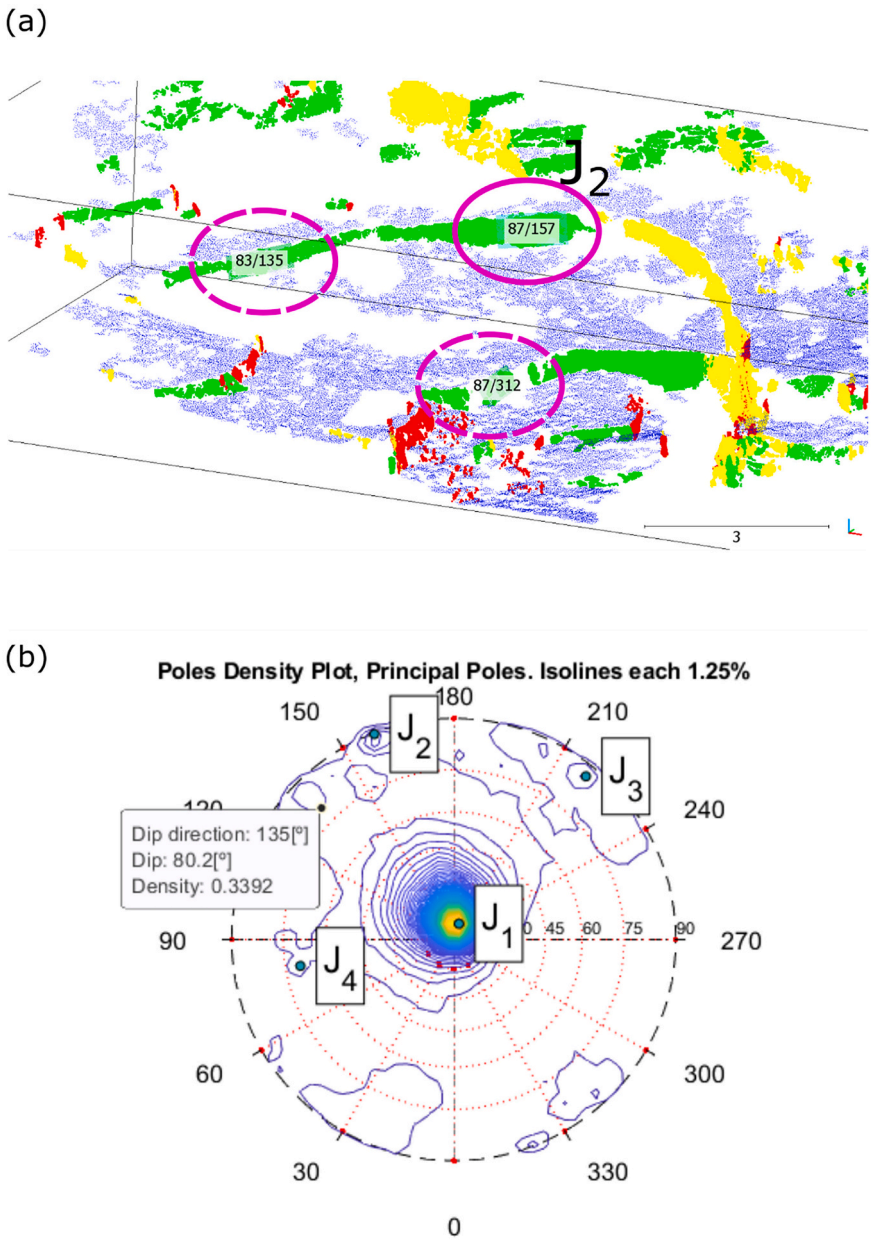

Fig. 13. (a) Orthographic view of the classified 3DPC of S01. J_2 data are shown in yellow. Purple ellipses show the areas of closely spaced J_2 data; (b) stereonet of the density of the poles showing the orientations extracted from (a). (For interpretation of the references to colour in this figure legend, the reader is referred to the web version of this article.)

Table 2
Summary of the detected DSs.

Sector	Type of plane	Detected DSt			
Sector 01	Natural fracture	J_1	J_2	J_3	J_4
	Front of extraction	J_1	–	J_3	J_4
Sector 03	Natural fracture	J_1	J_2	J_3	J_4
	Front of extraction	J_1	J_2	J_3	J_4

These results show that natural fractures were preferred for the traditional management of quarries in preindustrial times because the resulting extraction was easier. An analysis of the accurate orientations of the quarry fractures was carried out, revealing the use of natural discontinuities as planes of weakness.

We expect that future works will apply this method to both modern and historical quarries. For historical quarries, this method can contribute to increasing our geoarchaeological knowledge in conjunction with new methods and techniques. In addition, for modern quarries where minimising waste is required, this method will help manage the quarry by understanding the influences of natural fractures.

Author statement

Adrián Riquelme: Supervision, Conceptualization, Methodology, Fieldwork; Writing-Reviewing and Editing

Javier Martínez: Conceptualization, Fieldwork; Writing-Reviewing and Editing, Validation

Iván Martín-Rojas: Fieldwork; Writing-Reviewing and Editing, Validation

Roberto Sarro-Trigueros: Fieldwork, Reviewing

Álvaro Rabat: Reviewing

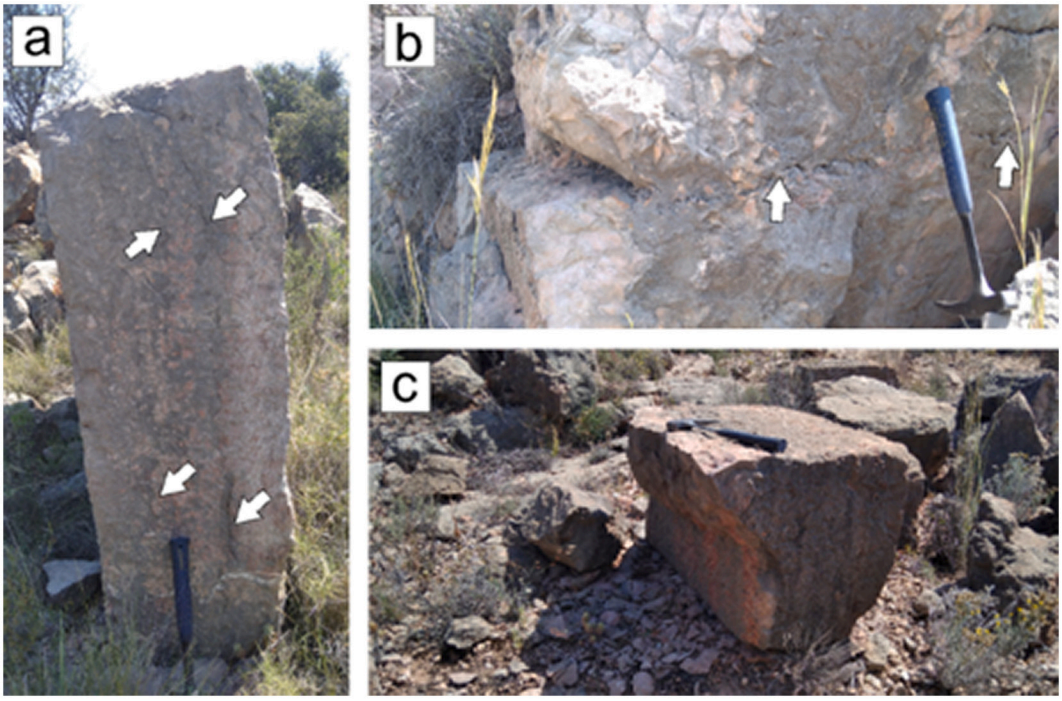

Fig. 14. Three examples of unfinished rock blocks: (a) rock block cut parallel to stylolite planes (white arrows); (b) wedge boxes along the surface trace of a stylolite (white arrows); (c) non-parallelepiped block partially reworked to obtain a regular ashlar.

Declaration of Competing Interest

The authors declare that they have no known competing financial interests or personal relationships that could have appeared to influence the work reported in this paper.

Acknowledgements

This research was funded by the Spanish Ministry of Economy and Competitiveness (MINECO) and EU FEDER under Project TEC2017-85244-C2-1-P, the University of Alicante (Vigrob-157 and GRE18-15), and the Spanish Ministry of Science and Innovation (Grants PID2020-116896RB-C21 and PID2020-116896RB-C22 funded by MCIN/AEI/10.13039/501100011033). The authors appreciate the stimulating conversations with Víctor Navarro-Fuster, PhD.

References

Agisoft, L.L.C., 2019. Agisoft Metashape Professional.

Anna Gutiérrez, G.M., 2011. The exploitation of local stone in Roman times: the case of north-eastern Spain. World Archaeol. 43, 318–341. https://doi.org/10.1080/00438243.2011.586201.

Assali, P., Grussenmeyer, P., Villemin, T., Pollet, N., Viguier, F., 2014. Surveying and modeling of rock discontinuities by terrestrial laser scanning and photogrammetry: Semi-automatic approaches for linear outcrop inspection. J. Struct. Geol. 66, 102–114. https://doi.org/10.1016/j.jsg.2014.05.014.

Bessac, J.-C., 2003. L'extraction des pierres de taille et des roches marbrières dans l'Antiquité: les principales stratégies d'exploitation. In: Marbres En Franche-Comté: Actes Des Journées d'étude. Association Pour La Promotion et Le Développement de l'Inventaire Comtoi, Besançon, pp. 21–34.

Bianchi Fasani, G., Bozzano, F., Cardarelli, E., Cercato, M., 2013. Underground cavity investigation within the city of Rome (Italy): a multi-disciplinary approach combining geological and geophysical data. Eng. Geol. 152, 109–121. https://doi.org/10.1016/J.ENGGEO.2012.10.006.

Botev, Z.I., Grotowski, J.F., Kroese, D.P., 2010. Kernel density estimation via diffusion. Ann. Stat. 38, 2916–2957. https://doi.org/10.1214/10-AOS799.

Donnelly, T., 1979. Structural and Technical Change in the Aberdeen Granite Quarrying Industry 1830–1880. Ind. Archaeol. Rev. 3, 228–238. https://doi.org/10.1179/iar.1979.3.3.228.

Einstein, H.H., Veneziano, D., Baecher, G.B., O'Reilly, K.J., 1983. The effect of discontinuity persistence on rock slope stability. Int. J. Rock Mech. Min. Sci. Geomech. Abstr. 20, 227–236. https://doi.org/10.1016/0148-9062(83)90003-7.

Ester, M., Kriegel, H., Sander, J., Xu, X., 1996. A density-based algorithm for discovering clusters in large spatial databases with noise. In: Simoudis, E., Han, J., Fayyad, U. (Eds.), Second International Conference on Knowledge Discovery and Data Mining. AAAI Press, Portland, Oregon, pp. 226–231.

Fant, J.C., 2012. Quarrying and Stoneworking. Oxford Handb. Eng. Technol. Class. World. https://doi.org/10.1093/oxfordhb/9780199734856.013.0006.

García-Sellés, D., Falivene, O., Arbués, P., Gratacos, O., Tavani, S., Muñoz, J.A., 2011. Supervised identification and reconstruction of near-planar geological surfaces from terrestrial laser scanning. Comput. Geosci. 37, 1584–1594. https://doi.org/10.1016/j.cageo.2011.03.007.

Grenne, T., Meyer, G.B., Heldal, T., Jansen, Ø.J., Løland, T., 2014. Technological development in millstone quarrying through the Middle Ages: the Salten quarries, Northern Norway. In: Seen through a Millstone, pp. 227–244.

Heldal, Tom, 2009. Constructing a quarry landscape from empirical data. General perspectives and a case study at the Aswan West Bank, Egypt. In: Abu-Jaber, N., Bloxam, E.G., Degryse, P., Heldal, T. (Eds.), QuarryScapes: Ancient Stone Quarry Landscapes in the Eastern Mediterranean, Geological Survey of Norway Special Publication, pp. 125–153.

Instituto Geográfico Nacional de España, 2016a. Centro de Descargas del CNIG (IGN) [WWW Document]. URL. http://centrodedescargas.cnig.es/CentroDescargas/catalogo.do#selectedSerie (accessed 12.28.16).

Instituto Geográfico Nacional de España, 2016b. Plan Nacional de Ortofotografía Aérea (PNOA) [WWW Document]. URL. http://pnoa.ign.es/presentacion (accessed 9.9.16).

ISRM, 1978. International Society for Rock Mechanics Commission on standardization of laboratory and field tests: Suggested methods for the quantitative description of discontinuities in rock masses. Int. J. Rock Mech. Min. Sci. Geomech. Abstr. 15, 319–368. https://doi.org/10.1016/0148-9062(79)91476-1.

Jaboyedoff, M., Oppikofer, T., Abellán, A., Derron, M.H.M.-H., Loye, A., Metzger, R., Pedrazzini, A., 2012. Use of LIDAR in landslide investigations: a review. Nat. Hazards 61, 5–28. https://doi.org/10.1007/s11069-010-9634-2.

Koch, L.J., Cardozo, N., Martin-Rojas, I., Alfaro, P., Castro, J., Medina-Cascales, I., García-Tortosa, F.J., 2017. 3D reconstruction of a normal fault zone - A trenching study on a strand of the active Baza Fault, South Central Spain. In: 79th EAGE Conference and Exhibition 2017: Energy, Technology, Sustainability - Time to Open a New Chapter. European Association of Geoscientists and Engineers, EAGE, University of Stavanger, Norway.

Lato, M.J., Diederichs, M.S., Hutchinson, D.J., 2010. Bias correction for view-limited Lidar scanning of rock outcrops for structural characterization. Rock Mech. Rock. Eng. 43, 615–628. https://doi.org/10.1007/s00603-010-0086-5.

Leica Geosystems, A.G., 2011. Leica ScanStation C10 Data Sheet. Heerbrugg, Switzerland.

Leica Geosystems, A.G., 2021. Cyclone 2021.1.2 64-bit.

Levytskyi, V., Sobolevskyi, R., Zawieska, D., Markiewicz, J., 2017. The accuracy of determination of natural stone cracks parameters based on Terrestrial Laser Scanning and dense image matching data. In: 17th International Multidisciplinary Scientific Conference SGEM2017. International Multidisciplinary Scientific

Geoconference, Albena; Bulgaria, pp. 255–262. https://doi.org/10.5593/sgem2017/23/S10.031.
Levytskyi, V., Sobolevskyi, R., Korobiichuk, V., 2018. The optimization of technological mining parameters in a quarry for dimension stone blocks quality improvement based on photogrammetric techniques of measurement. Rud. Geol. Naft. Zb. 33, 83–89. https://doi.org/10.17794/rgn.2018.2.8.
Luhmann, T., Robson, S., Kyle, S., Boehm, J., 2019. Close-Range Photogrammetry and 3D Imaging, Close-Range Photogrammetry and 3D Imaging. De Gruyter. https://doi.org/10.1515/9783110607253.
Martínez-Martínez, J., 2020. Apuntes para la reconstrucción del panorama cantero en el Medio Vinalopó (Alicante) previo a la eclosión y comercialización de la 'piedra de Novelda' a nivel nacional. In: Paisajes e Historias En Torno a La Piedra. Universidad Nacional de Educación a Distancia (España), pp. 467–488. https://doi.org/10.5944/monografias.prehistoria.arqueologia.2020.15.
Martínez-Martínez, J., Corbí, H., Martin-Rojas, I., Baeza-Carratalá, J.F., Giannetti, A., 2017. Stratigraphy, petrophysical characterization and 3D geological modelling of the historical quarry of Nueva Tabarca island (western Mediterranean): Implications on heritage conservation. Eng. Geol. 231, 88–99. https://doi.org/10.1016/j.enggeo.2017.10.014.
Medina-Cascales, I., Koch, L., Cardozo, N., Martin-Rojas, I., Alfaro, P., García-Tortosa, F. J., 2019. 3D geometry and architecture of a normal fault zone in poorly lithified sediments: a trench study on a strand of the Baza Fault, central Betic Cordillera, South Spain. J. Struct. Geol. 121, 25–45. https://doi.org/10.1016/j.jsg.2019.02.003.
Mosch, S., Nikolayew, D., Ewiak, O., Siegesmund, S., 2011. Optimized extraction of dimension stone blocks. Environ. Earth Sci. 63, 1911–1924. https://doi.org/10.1007/s12665-010-0825-7.
Niethammer, U., James, M.R., Rothmund, S., Travelletti, J., Joswig, M., 2012. UAV-based remote sensing of the Super-Sauze landslide: Evaluation and results. Eng. Geol. 128, 2–11. https://doi.org/10.1016/j.enggeo.2011.03.012.
Nieto, L.M., Reolid, M., Molina, J.M., Ruiz-Ortiz, P.A., Jiménez-Millán, J., Rey, J., 2012. Evolution of pelagic swells from hardground analysis (Bathonian-Oxfordian, Eastern External Subbetic, southern Spain). Facies 58, 389–414. https://doi.org/10.1007/s10347-011-0281-1.
Priest, S.D., Hudson, J.A., 1976. Discontinuity spacings in rock. Int. J. Rock Mech. Min. Sci. Geomech. Abstr. 135–148. https://doi.org/10.1016/0148-9062(76)90818-4.
Priest, S.D., Hudson, J.A., 1981. Estimation of discontinuity spacing and trace length using scanline surveys. Int. J. Rock Mech. Min. Sci. 18, 183–197. https://doi.org/10.1016/0148-9062(81)90973-6.
Reolid, M., Nieto, L.M., 2010. Jurassic Fe-Mn macro-oncoids from pelagic swells of the External Subbetic (Spain): evidences of microbial origin. Geol. Acta 8, 151–168. https://doi.org/10.1344/105.000001525.
Riquelme, A., 2015. Uso de nubes de puntos 3D para identificación y caracterización de familias de discontinuidades planas en afloramientos rocosos y evaluación de la calidad geomecánica. Universidad de Alicante doi.org/http://hdl.handle.net/10045/51107.
Riquelme, A., Abellán, A., Tomás, R., Jaboyedoff, M., 2014a. A new approach for semi-automatic rock mass joints recognition from 3D point clouds. Comput. Geosci. 68, 38–52. https://doi.org/10.1016/j.cageo.2014.03.014.
Riquelme, A., Abellán, A., Tomás, R., Jaboyedoff, M., 2014b. Rock slope discontinuity extraction and stability analysis from 3D point clouds: application to an urban rock slope. In: Vertical Geology, from Remote Sensing to 3D Geological Modelling. Proceedings of the First Vertical Geology Conference. University of Lausanne, pp. 75–78.
Riquelme, A., Abellán, A., Tomás, R., 2015. Discontinuity spacing analysis in rock masses using 3D point clouds. Eng. Geol. 195, 185–195. https://doi.org/10.1016/j.enggeo.2015.06.009.
Riquelme, A., Tomás, R., Cano González, M., Abellán, A., 2016. Using open-source software for extracting geomechanical parameters of a rock mass from 3D point clouds: Discontinuity Set Extractor and SMRTool. In: Ulusay, R., Aydan, Ö., Gerçek, H., Hindistan, M., Tuncay, E. (Eds.), Rock Mechanics & Rock Engineering: From the Past to the Future. CRC Press. Taylor & Francies Group, London, pp. 1091–1096.
Riquelme, A., Cano González, M., Tomás, R., Abellán, A., 2017. Identification of rock slope discontinuity sets from laser scanner and photogrammetric point clouds: a comparative analysis. In: Procedia Engineering, pp. 838–845. https://doi.org/10.1016/j.proeng.2017.05.251.
Riquelme, A., Tomás, R., Cano González, M., Pastor, J.L., Abellán, A., 2018. Automatic mapping of discontinuity persistence on rock masses using 3D point clouds. Rock Mech. Rock. Eng. 51, 3005–3028. https://doi.org/10.1007/s00603-018-1519-9.
Rocscience, 2021. Dips (Build 8.013 64bits).
Scard, A.M., 1989. The Development and changing Organisation of Shropshire's Quarrying Industry: 1750-1900. Ind. Archaeol. Rev. 11, 171–186. https://doi.org/10.1179/iar.1989.11.2.171.
Slob, S., van Knapen, B., Hack, H.R.G.K., Turner, K., Kemeny, J., 2005. Method for automated discontinuity analysis of rock slopes with three-dimensional laser scanning. Transp. Res. Rec. 1913, 187–194. https://doi.org/10.3141/1913-18.
Slob, S., Turner, A., Bruining, J., Hack, H.R.G.K., 2010. Automated Rock Mass Characterisation Using 3-D Terrestrial Laser Scanning. Delft University of Technology, TU Delft https://doi.org/0166077.
Smith, M.J., Chandler, J., Rose, J., 2009. High spatial resolution data acquisition for the geosciences: Kite aerial photography. Earth Surf. Process. Landf. 34, 155–161. https://doi.org/10.1002/esp.1702.
Stanier, P., 1985. The granite quarrying industry in Devon and Cornwall Part One 1800-1910. Ind. Archaeol. Rev. 7, 171–189. https://doi.org/10.1179/iar.1985.7.2.171.
Stumpf, A., Malet, J.P., Kerle, N., Niethammer, U., Rothmund, S., 2013. Image-based mapping of surface fissures for the investigation of landslide dynamics. Geomorphology 186, 12–27. https://doi.org/10.1016/j.geomorph.2012.12.010.
Sturzenegger, M., Stead, D., 2009. Quantifying discontinuity orientation and persistence on high mountain rock slopes and large landslides using terrestrial remote sensing techniques. Nat. Hazards Earth Syst. Sci. 9, 267–287.
Tallon, A., 2014. Divining proportions in the information age. Archit. Hist. 2, 15. https://doi.org/10.5334/AH.BO.
Vasuki, Y., Holden, E.J., Kovesi, P., Micklethwaite, S., 2014. Semi-automatic mapping of geological Structures using UAV-based photogrammetric data: an image analysis approach. Comput. Geosci. 69, 22–32. https://doi.org/10.1016/j.cageo.2014.04.012.
Vöge, M., Lato, M.J., Diederichs, M.S., 2013. Automated rockmass discontinuity mapping from 3-dimensional surface data. Eng. Geol. 164, 155–162. https://doi.org/10.1016/j.enggeo.2013.07.008.